Time resolved evolution of structural, electrical, and thermal properties of copper irradiated by an intense ultrashort laser pulse

Arvinder S. Sandhu,[a] A. K. Dharmadhikari, and G. Ravindra Kumar
Tata Institute of Fundamental Research, 1 Homi Bhabha Road, Colaba, Mumbai, India 400005

(Received 30 August 2004; accepted 28 October 2004; published online 27 December 2004)

The dynamical properties of copper metal are obtained on a picosecond time scale using 100 fs laser pulse at 10^{15} W cm^{-2}—an intensity regime relevant to femtosecond micromachining. The dissipation mechanisms and scaling laws spanning a wide temperature range are obtained from femtosecond pump–probe reflectivity. We observe obliteration of the crystalline structure in copper within 400 fs due to lattice disorder caused by the intense laser pulse. The electrical resistivity is obtained by studying the probe reflectivity evolution from 0 to 30 ps. The "resistivity saturation" effect in an unexplored regime intermediate to hot plasma and cold solid is studied in detail. The temperature evolution and thermal conductivity values are also obtained. © *2005 American Institute of Physics*. [DOI: 10.1063/1.1834726]

I. INTRODUCTION

The availability of femtosecond lasers has sparked considerable work in both fundamental and applied physics. There has been a great deal of interest in understanding the evolution of a solid that is impulsively heated by a subpicosecond laser pulse, thereby creating highly nonequilibrium conditions.[1,2] Substantial understanding of the electronic properties of solids in nonequilibrium and short time scale regimes has come from relatively low intensity ($\sim 10^{12}$ W cm^{-2}) experiments.[3–6] At sufficiently high intensity, phenomena like ultrafast phase transitions, thermal, and nonthermal structural transformations and melting dynamics have been attracting significant attention.[7–10] In the "high intensity" regime, ultrashort laser pulses have been instrumental in understanding the properties of solid plasmas under conditions of extreme temperatures and high densities[11,12] that resemble stellar interior conditions. The dynamics of solid evolution for laser pulse intensities $\geqslant 10^{14}$ W cm^{-2} has immediate importance in view of the increasing application of femtosecond laser pulses for precision micromachining and material processing.[13–15]

As a general framework, it has been established that when a short laser pulse hits a solid, the electrons are elevated to 1–2 orders higher temperature than the lattice.[1,2] Within the electron subsystem the energy exchange timescales are of the order of 10^{-14} s for $T_e > 1$ eV; thus electrons are in local thermodynamic equilibrium and can be characterized by a single temperature value. Strongly coupled ions can also be similarly described by a single temperature value. Thus, the situation can be approximately modeled as a two-temperature nonequilibrium system. The understanding of laser energy absorption under such situations is crucial as it can help determine electron and thermal transport, equation of state, structural properties, and phase transitions. As the energy deposition by the pump laser occurs very rapidly the temperature is expected to reach 50–100 eV before any bulk motion of target material can take place. Thereafter the interplay of lattice and electron dynamics collectively decides the behavior of the material. This makes the modeling of thermal and electrical conductivity both complex and highly interesting from the physics point of view. To our knowledge, there exists no general theoretical formalism to encompass the transition from hot plasma to cold solid over picosecond timescales. Time resolved reflectivity is thus a powerful tool to extract dynamical information about such nonequilibrium systems. A very interesting example of the application of time resolved reflectivity is the demonstration and measurement of the properties of the fluid phase of carbon, which exists only in very high temperature and pressure regimes.[16]

Here, we determine the electrical and thermal properties of copper using time resolved femtosecond pump–probe reflectivity to study the entire range of evolution from hot plasma to a cold solid. We address the question of time taken for the disintegration of regular crystalline structure of the solid after interaction with intense ultrashort laser pulse. We monitor the interband absorption in copper to establish a time scale for lattice disordering. We classify our study of time resolved reflectivity into three temperature regimes, namely, high temperature hot plasma limit, low temperature limit, and the intermediate case. We carry out a time resolved study to establish the mechanisms of energy damping and temperature scaling of various processes over the time scale 0–30 ps. We obtain the evolution of collision frequency (which determines laser energy dissipation), dc-electrical resistivity, and thermal conductivity as a function of time and electron temperature. We observe that the collision frequency (ν) scales as $T_e^{-3/2}$ in the hot plasma limit, as expected, where T_e is the electron temperature. For very low temperature equilibrium conditions, dissipation is expected to arise from electron–phonon collisions mainly and $\nu \propto T_i$, where T_i is ion temperature. However, when the electron temperature is more than the Fermi temperature and ion temperature, electron–electron scattering, which goes as T_e^2, is generally assumed to dominate over the electron–phonon

[a]Present address: JILA, University of Colorado, Boulder, CO 80309; electronic address: arvinder@jila.colorado.edu

contribution.[17–19] We verify this phenomenon experimentally under the above temperature conditions. The intermediate transition regime exhibits the phenomenon of "resistivity saturation," where the electron mean free path becomes of the order of interparticle spacing. In this intermediate temperature regime our results on electrical resistivity and thermal conductivity are different in the sense that there exist no established scaling laws to estimate material properties in this regime. The difficulty in understanding the intermediate regime stems from the fact that one cannot use a simple weakly coupled plasma description and the collision frequency has to be determined rigorously, taking care of strong coupling between electrons as well as between ions.[20]

II. GOVERNING EQUATIONS

The behavior of a metal under the action of laser pulse, i.e., energy absorption processes, and the concomitant evolution of electron and ion temperature, can be modeled by the following set of equations:[2]

$$C_e(T_e)\frac{\partial T_e}{\partial t} = \kappa \nabla^2 T_e - g(T_e - T_i) + A(r,t), \tag{1}$$

$$C_i \frac{\partial T_i}{\partial t} = g(T_e - T_i), \tag{2}$$

$$\frac{d^2E}{dx^2} + k^2(n^2 - \sin^2\theta)E = 0, \tag{3}$$

$$\frac{d^2B}{dx^2} + k^2(n^2 - \sin^2\theta)B - i\frac{4\pi}{ckn^2}\frac{d\sigma}{dx}\frac{dB}{dx} = 0. \tag{4}$$

Equations (1) and (2) are coupled equations for the electron and ion temperatures, respectively. Here C_e (C_i) is electron (ion) heat capacity, g is electron–phonon coupling constant, κ is thermal conductivity, and A represents the laser energy absorption. Equations (3) and (4) are Helmoltz equations for propagation of *s*- and *p*-polarized laser pulses, respectively, in a finite scale length density gradient inside the metal. The refractive index n for Drude (intraband) absorption is of the form, $n^2 = 1 + i4\pi\sigma/\omega$; ω is the laser frequency and σ is the conductivity given by $\sigma = 1/4\pi(\nu + i\omega)[\omega_p^2/(\omega^2 + \nu^2)]$, where $\omega_p = 4\pi n_e e^2/m_e$, the plasma frequency.

III. EXPERIMENT

For our experiment we obtain high intensity (3×10^{15} W/cm^2, 100 fs, 806 nm) pulses from a custom built chirped pulse amplification Ti:S laser which is described in detail elsewhere.[21] A small part of the laser light is frequency doubled in a thin BBO crystal to produce a 403 nm probe pulse. The laser pulse contrast ratio was 10^{-5} at 1 ps for the fundamental and is expected to be 10^{-10} for the second harmonic probe. The targets used in these experiments were polished metal discs with flatness better than $\lambda/5$. The delay between pump and probe is changed in small steps using a precision translation stage. The pump and probe spot sizes were 30 and 20 μm respectively. The incident pump is *p* polarized and incident at 50° with respect to the target normal. The 403 nm probe is at near normal incidence ($<5°$) and is also *p* polarized. The probe intensity is 10^{12} W cm^{-2}, i.e., 3000 times weaker than the pump. In the data presented here we monitored the temporal behavior of probe reflectivity from −5 to +30 ps time delay. The reflectivity of the probe was found to remain specular within our range of interest. This was checked by collecting light from nonspecular directions onto a photodiode and monitoring the signal as a function of time delay. Two similar photodiodes were used to measure the specularly reflected laser energy and input laser energy variation, respectively. The pump–probe reflectivity was obtained for copper. Copper is not a "simple metal" like aluminum and has not been studied in this intensity and temporal regime. Aluminum reflectivity is, however, also obtained here to serve as a comparison with copper.

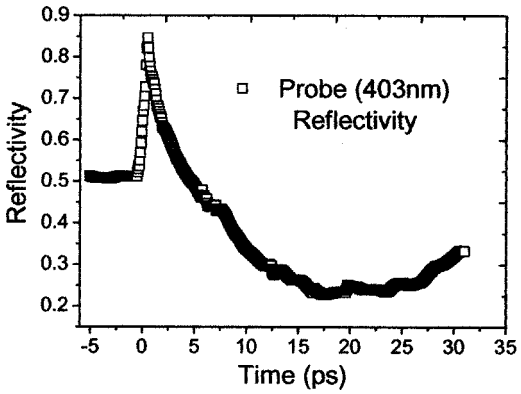

FIG. 1. Time resolved reflectivity of probe ($\lambda = 403$ nm, $I = 10^{12}$ W cm^{-2}) from copper irradiated by 3×10^{15} W cm^{-2}, 806 nm pump pulse incident at 50°.

IV. RESULTS AND DISCUSSION

Figure 1 shows the time resolved reflectivity of a weak 403 nm probe from metal irradiated by 806 nm, 3×10^{15} W cm^{-2} pump laser. On the negative delay side, where the probe is ahead of the pump, the reflectivity is 50%, which is the same as room temperature reflectivity of copper at 403 nm. The low value of reflectivity is due to strong interband ($3d$-$4p$) absorption in copper. In comparison, aluminum behaves as a simple metal at 403 nm, and has 92% reflectivity at negative delay (Fig. 2). The absorption in alu-

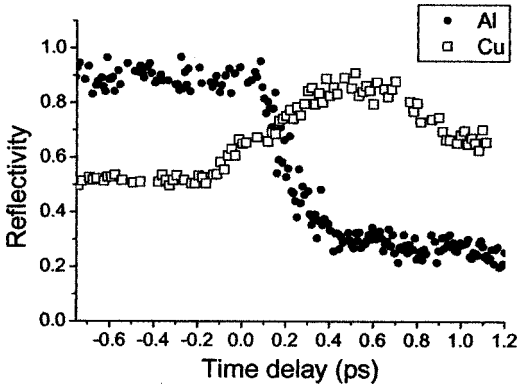

FIG. 2. The higher resolution reflectivity for copper and its comparison with aluminum near zero time delay position.

minum is solely due to *interband* transitions (Drude model), whereas *intraband* transitions play a prominent role in copper. The interesting feature of Copper reflectivity is the sharp rise near zero delay (Fig. 1). In order to understand this better we also carried out higher resolution runs for both copper and aluminum near zero delay and raw data are shown in Fig. 2. In the case of copper we see a sharp rise from 0.5 to almost 0.9 in about 400 fs, and then reflectivity starts to decrease again. In aluminum, reflectivity rather than showing any increase shows expected Drude behavior and falls rapidly from 0.9 to 0.3 in about 400 fs, thereafter followed by a slower decrease. The reason for the sharp increase in copper is thus related to interband transitions because any other effect related to intraband or Drude absorption should have been similar in both metals. Thus, we here isolate the effect of intense laser irradiation on the band structure of a solid, which is a measure of crystalline order. Near the zero delay position, metal experiences intense conditions that lead to high temperatures and ionization. One can expect these strong excitation conditions to induce lattice instability, which grows very fast and leads to complete suppression of interband absorption processes. Increasing temperature by itself can lead to larger separation of the atomic levels, and, hence reduced $3d$-$4p$ absorption.[12] The sharp reflectivity change from 0.5 to 0.9 is thus a clear demonstration of the disintegration of regular crystalline order in a metal induced by intense ultrashort laser pulse. Our results in Fig. 2 show that the time taken for complete loss of order is 400 fs, i.e., more than the pulse width of the laser pulse. The lattice structure is also disordered to some extent via an ultrafast melting process, but that is not the major mechanism as discussed below.

At the peak of probe reflectivity the pump laser has completely vanished, leaving behind a hot ($\sim$50 eV), expanding plasma. Now intraband or Drude processes basically govern the absorption in the plasma. In this regime the temperature and collision frequency will change with time, and together with increasing length scale, will result in reflectivity behavior as shown in Fig. 1. For quantitative understanding we numerically solved the Helmoltz equation, following Milchberg and Freeman,[22] for the p-polarized probe propagating inside hot evolving plasma. The atomic density profile is assumed to be parabolic, of the form $N=N_0(1-x/L)^2$, where N_0 is the atomic density of the solid. The electron density is determined using $n_e(x)=n_{\text{solid}}N(x)/N_0$. As indicated in Ref. 22, the calculation for reflectivity does not vary much between this method and using the local thermodynamic equilibrium method to deduce n_e from N and T_e. The plasma scale length $L(t)$ is estimated from Doppler shift measurements of the probe and is also consistent with electron temperature profiles discussed later. The collision frequency is also assumed to be dependent on x via the functional form $\nu/\omega \propto (1-x/L)^2$. Then for each reflectivity value, we solve Eq. (4) above for the value of collision frequency parameter ν needed to get corresponding reflectivity at that instant of time as shown in Fig. 3 (x axis on top and y axis on right). The collision frequency is seen to first increase fast from 6×10^{15} to 1.5×10^{16} s^{-1}, in a span of 1–3 ps. Then it shows a broad plateau (3–15 ps) before falling off again. We use

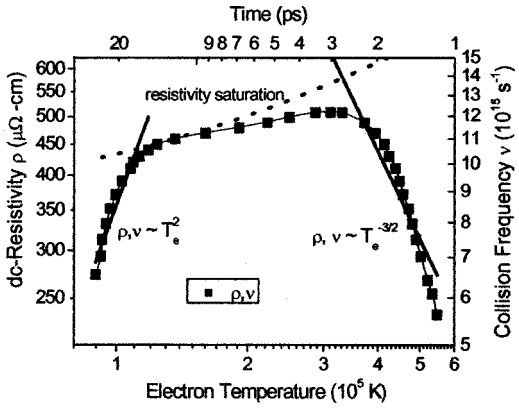

FIG. 3. The electrical resistivity and collision frequency as a function of time delay (top axis) and electron temperature (bottom axis). The solid lines are for appropriate scaling laws and the dotted curve is the theoretical upper bound on resistivity.

the collision frequency information to deduce the dc resistivity ρ_{dc}, a more important and commonly used parameter that is related to collision frequency as $\rho_{\text{dc}}=\nu m/n_e e^2$. This, and other parameters henceforth, were obtained at an electron density equivalent to a solid density of 8.47×10^{22} cm^{-3}. The resistivity obtained varies between 200 and 500 $\mu\Omega$ cm in the same fashion as collision frequency. The regime of broad maxima is called the resistivity saturation regime.[23] Before discussing resistivity further it is very useful to estimate electron and ion temperatures corresponding to time scales involved. For the evolution of temperature we solve coupled diffusion equations for electron and ion temperatures. The thermal conductivity κ is taken to be of the form[24] $\kappa=\kappa_0(T_e/\nu)$, where $\kappa_0=7.5\times10^{13}$ Jm^{-1} K^{-2}, obtained as in Ref. 25. The electron specific heat C_e varies as 96.6 T_e Jm^{-3} K^{-1} at low temperatures[5] and as 1.5 $k_B n_e$ at high temperatures.[18] We use harmonic interpolation for intermediate temperatures. The ion specific heat $C_i=3\ k_B n_i$ and coupling constant g is taken[25] as 10^{17} Wm^{-3} K^{-1}. The laser energy absorption is incorporated assuming a Gaussian intensity profile of the laser pulse with the half width of 100 fs. The resulting electron and ion temperature profiles at solid density are shown in Fig. 4. The approximation we use here for electron and ion specific heat modeling is somewhat crude, but in absence of the exact knowledge of the specific

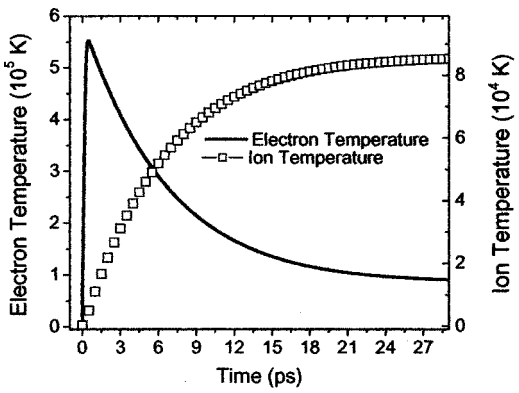

FIG. 4. The electron (line) and ion (open squares) temperature evolution as a function of time delay.

heat behavior these approximations are widely used under temperature and intensity conditions similar to ours.[18] However, despite this fact, the main conclusions of this work are unaffected, as we here illustrate the fundamental concepts and scaling of short pulse matter interaction in different regimes. The electron temperature sharply increases to about 50 eV in less than a picosecond while ions are still two orders of magnitude lower in temperature, thus resulting in a highly nonequilibrium situation. The dynamics after the pump pulse is determined by electron lattice coupling and electron thermal conductivity. As seen from Fig. 4, the electron temperature decreases fast, and substantial equilibration of the electron-ion system takes place in 25 ps. It is interesting to note that the ion temperature reaches melting temperature of copper before the intensity maximum of the pump pulse is reached. This is expected at our laser intensity. Thus the structural changes due to "ultrafast melting" that occur on the rising edge of the pump laser pulse can also contribute to decrease of interband absorption near zero delay. However, that alone cannot obliterate band structure, as evidenced by the relatively large absorption at 100 fs duration as shown in Fig. 2. This is indicative of the fact that ion correlations are preserved to a sufficient extent even in the transition from a solid to a liquid state occurring on a very short time scale.

We obtain the bottom axis for Fig. 3 using T_e as a function of time from Fig. 4. Thus we now obtain dc-electrical resistivity and collision frequency as a function of both electron temperature and time. Two limiting cases can be clearly seen within our study, a high temperature limit where resistivity falls with temperature from 500 $\mu\Omega$ cm to 200 $\mu\Omega$ cm and a low temperature limit where resistivity rises with increasing temperature. This is not unexpected as in the hot plasma limit where $T_e \gg E_F/k_B$ (E_F is Fermi energy), the collision frequency and, hence, the resistivity goes almost as $T_e^{-3/2}$. The solid line on the right side of the graph indicates the exact $T_e^{-3/2}$ behavior. At the lower temperature side ($T_e \sim E_F/k_B$), the resistivity varies as T_e^2 (solid line on the right side of Fig. 3). This indicates that the electron–electron scattering, which goes as T_e^2, dominates over the electron phonon scattering, which should vary as T_i. However, it is important to note that the system spends most of its time (3–15 ps) in the intermediate temperature regime, thus making this regime even more important.

The intermediate transition regime shows very little variation and represents saturation of resistivity around 450 $\mu\Omega$ cm. The maximum value for resistivity (collision frequency) can be determined by the condition that the mean free path λ_e, between two collisions is greater than the interparticle distance r_0, which can be calculated as $(3/4\pi n_e)^{1/3}$. This condition can also be written as $\nu \leqslant V_e/r_0$, where V_e is the characteristic electron velocity, and can be deduced from, $V_e = \sqrt{V_{\mathrm{Fermi}} + k_B T_e/m}$; V_{Fermi} is the Fermi velocity. The estimated maximum of ν and ρ is plotted in Fig. 3 as the dotted line. The experimental saturation behavior is evidently in good agreement with this simple theoretical estimate for maximum of resistivity.

The thermal conductivity $\kappa = \kappa_0(T_e/\nu)$, which was deduced above, is as shown in Fig. 5. The high temperature

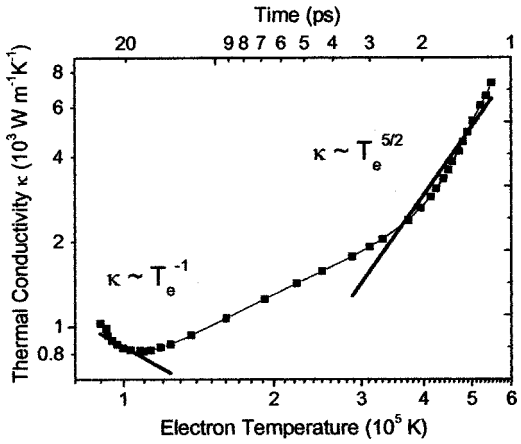

FIG. 5. Thermal conductivity deduced as a function of time delay and electron temperature. The higher and lower end scaling is shown as solid lines.

shows the expected behavior $\sim T_e^{5/2}$. On the lower side of the temperature scale, κ goes as T_e^{-1}, again as expected from $\kappa \propto T_e/\nu$. In order to observe the scaling as T_e/T_i, i.e., where electron–phonon interaction starts dominating momentum relaxation, one has to access even lower temperatures.

V. CONCLUSION

In conclusion, time resolved pump–probe reflectivity has enabled us to measure the time duration for the structural disintegration process to be approximately four times the laser pulse width. We have deduced the collision frequency, the dc-electrical resistivity, electron and ion temperature evolution, and thermal conductivity of a solid irradiated by an intense ultrashort laser pulse. At high temperatures, the collision frequency goes as $T_e^{-3/2}$, as expected for a hot plasma. At lower temperatures we establish the importance of electron–electron scattering, which goes as T_e^{-2}, as the principle energy dissipation mechanism over electron–phonon scattering. The behavior of metals in the intermediate, unexplored, temperature regime is obtained in detail. The saturation resistivity value ($\sim$450 $\mu\Omega$ cm) in the intermediate regime agrees well with theoretical estimates. We believe that knowledge of temperature and time dependent evolution of these parameters would be useful for emerging applications that involve the use of ultrashort laser interaction with metals.

ACKNOWLEDGMENTS

The authors thank Sudip Sengupta and P. K. Kaw for discussions and valuable help in numerical codes. The authors also thank P. P. Rajeev, Vinod Kumarappan, M. Krishnamurthy, and D. Mathur for useful suggestions. The laser system used was funded in part by the Department of Science and Technology, Government of India.

[1] S. I. Anisimov, B. L. Kapeliovich, and T. L. Perel'man, Sov. Phys. JETP **39**, 375 (1974).
[2] R. W. Schoenlein, W. Z. Lin, J. G. Fujimoto, and G. L. Eesley, Phys. Rev. Lett. **58**, 1680 (1987).
[3] C.-K. Sun, F. Vallee, L. H. Acioli, E. P. Ippen, and J. G. Fujimoto, Phys. Rev. B **50**, 15337 (1994).

[4]C. Guo, G. Rodriguez, and A. J. Taylor, Phys. Rev. Lett. **86**, 1638 (2001).
[5]H. E. Elsayed-Ali, T. B. Norris, M. A. Pessot, and G. A. Mourou, Phys. Rev. Lett. **58**, 1212 (1987).
[6]J. Hohlfeld, J. G. Muller, S.-S. Wellershoff, and E. Matthias, Appl. Phys. B: Lasers Opt. **64**, 387 (1997).
[7]K. Sokolowski-Tinten, C. Blome, C. Dietrich, A. Tarasevich, M. Horn von Hoegen, D. von der Linde, A. Cavalleri, J. Squire, and M. Kammler, Phys. Rev. Lett. **87**, 225701 (2001).
[8]C. V. Shank, R. Yen, and C. Hirlimann, Phys. Rev. Lett. **50**, 454 (1983).
[9]S. I. Kudryashov and V. I. Emel'yanov, JETP Lett. **73**, 551 (2001).
[10]B. Rethfeld, K. Sokolowski-Tinten, D. von der Linde, and S. I. Anisimov, Phys. Rev. B **65**, 092103 (2002).
[11]W. Theobald, R. Häßner, R. Kingham, R. Sauerbrey, R. Fehr, D. O. Gericke, M. Schlanges, W.-D. Kraeft, and K. Ishikawa, Phys. Rev. E **59**, 3544 (1999).
[12]D. F. Price, R. M. More, R. S. Walling, G. Guethlein, R. L. Shepherd, R. E. Stewart, and W. E. White, Phys. Rev. Lett. **75**, 252 (1995).
[13]E. N. Glezer and E. Mazur, Appl. Phys. Lett. **71**, 882 (1997).
[14]M. D. Perry, B. C. Stuart, P. S. Banks, D. Fiet, V. Yanovsky, and A. M. Ribenchuk, J. Appl. Phys. **85**, 6903 (1999).
[15]R. Le Harzic, N. Huot, E. Audouard, C. Jonin, P. Laporte, S. Valette, A. Fraczkiewicz, and R. Fortunier, Appl. Phys. Lett. **80**, 3886 (2002).
[16]D. H. Reitze, H. Ahn, and M. C. Downer, Phys. Rev. B **45**, 2677 (1992).
[17]A. A. Abrikosov, *Introduction to the Theory of Normal Metals* (Academic Press, New York, 1972).
[18]D. Fisher, M. Fraenkel, Z. Henis, E. Moshe, and S. Eliezer, Phys. Rev. E **65**, 016409 (2001).
[19]A. P. Kanavin, I. V. Smetanin, V. A. Isakov, Yu. V. Afanasiev, B. N. Chichkov, B. Wellegehausen, S. Nolte, C. Momma, and A. Tunnermann, Phys. Rev. B **57**, 14698 (1998).
[20]S. Kato, R. Kawakami, and K. Mima, Phys. Rev. A **43**, 5560 (1991).
[21]P. P. Rajeev, S. Banerjee, A. S. Sandhu, R. C. Issac, L. C. Tribedi, and G. Ravindra Kumar, Phys. Rev. A **65**, 052903 (2002).
[22]H. M. Milchberg and R. R. Freeman, J. Opt. Soc. Am. B **6**, 1351 (1989).
[23]H. M. Milchberg, R. R. Freeman, S. C. Davey, and R. M. More, Phys. Rev. Lett. **61**, 2364 (1988).
[24]P. B. Corkum, F. Brunel, N. K. Sherman, and T. Srinivasan Rao, Phys. Rev. Lett. **61**, 2886 (1988).
[25]K. Eidmann, J. Meyer-ter-Vehn, T. Schlegel, and S. Huller, Phys. Rev. E **62**, 1202 (2002).